LPV techniques for the control of an airborne micro-launcher

J. Bordeneuve-Guibé, D. Alazard *
J. Desmariaux †

Abstract

This paper addresses the robust control of a micro-launcher. The general framework of this work is a R&D project of the French space agency (CNES) focused on new launchers. The objective was to evaluate the potentialities of Linear Parameter Varying (LPV) techniques for the specific problem of launchers control. As a realistic test case, the micro-launcher preliminary research program, supported by the CNES Launcher Directorate, has been considered.

First a Linear Fractional Transformation (LFT) based model of the launcher has been established and validated. Then two strategies have been chosen to design a robust controller of the angle of attack: a complete LPV controller has first been developed; then a controller based on an LFT representation of a classical lead phase controller has been considered. Realistic simulations have been conducted to compare both strategies with a more traditional interpolated lead phase controller. Finally, the simulation results exhibit very promising results, allowing a total respect of the performance specifications.

Keywords

Robust Control, LPV systems, Guidance and Control, Aerospace vehicles, Launchers

1 Introduction

The development of new micro-satellites is a challenging problem by many aspects, especially because many types of launchers can be considered: In particular, a special attention is actually given to the solution consisting in launching payloads using light conventional fighter aircrafts. At a given altitude, the airborne micro-launcher is dropped from the aircraft and then initiates its flight until it reaches its orbit. This flight phase is crucial because the micro-launcher has to be controlled in incidence despite highly varying conditions (evolution of mass, velocity, dynamic pressure, etc.) and disturbances (wind shears). Moreover uncertainties on dropping conditions and mission objectives could lead to apply a closed-loop guidance control law in atmospheric phase, and the control loop would then have to cover a wide flight envelope by comparison with classical launchers. Considering this particular context, it is obvious that conventional controllers are not well suited to guaranty desired stability margins and performance levels along the whole trajectory. In particular, the controller parameters have to be made variable

*ISAE, Université de Toulouse, 10 avenue Edouard Belin, 31055 Toulouse Cedex 4, France. e-mail: joel.bordeneuve@isae.fr

†CNES, Rond Point de l'Espace, 91023 Evry, France.

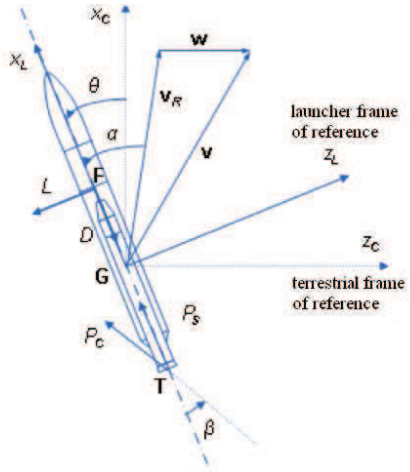

Figure 1: Reference frames and variables of interest

and adaptable to flight conditions. A practical approach consists in tuning and scheduling various LTI (Linear Time Invariant) controllers designed in various flight conditions. But linear parameters varying (LPV) techniques are now mature enough to offer both theoretical and applied solutions. Concerning aerospace systems, LPV system modeling has been extensively studied [1], and efficient frameworks are now available [2]. More recent developments [3] address the direct design of a LPV controller from a Linear Fractional Representation (LFR) of the parameter dependant model. Moreover, dedicated Matlab toolboxes ([4], [5]) now offer an efficient design and simulation framework for complex systems.

First a complete linear model has been established between the input command (thruster's deflection) and the output angles (incidence, pitch). This model comes from the linearization of the rigid body launcher at the maximum dynamic pressure that represents the worst case along the flight trajectory. Then a classical lead phase discrete-time controller has been tuned to cope with the desired performance specifications (stability margins, damping factor and bandwidth). The next step has consisted in developing an appropriate LFT model: it has been shown that considering only Mach number and dynamic pressure, a convenient LFT model could be validated along the whole trajectory. Designing a control law using a direct LPV approach has resulted in a tough task, exhibiting encouraging simulation results. Then an alternative control law based on a LPV representation of the classical lead phase controller has been established. Simulations have been performed in a realistic context, i.e. taking into account the nonlinear and non-stationary characteristics of the micro-launcher.

2 LINEAR MODEL OF THE LAUNCHER

In order to develop a model of the micro-launcher, the variables of interest (Fig. 1) are the angle of attack (α), the pitch angle (θ), the thruster deflection (β). The terrestrial reference frame is denoted (X_C, Y_C, Z_C) while the frame attached to the launcher is (X_L, Y_L, Z_L). V and V_R vectors denote the velocity with respect to the ground and the air respectively; thus W, the difference between V and V_R is the wind vector. Lift (L) and drag (D) forces apply at the center of lift (F). G is the center of gravity and P_C is the total thrust force applying at T.

The model has been established under several classical assumptions concerning the launcher geometry, the airflow, the nature of the fluid and so on. Moreover, as wind is supposed to remain

small with respect to both absolute (V) and relative (V_R) velocities, the angle of attack (AoA) equation is:

$$\alpha = \theta + \frac{\dot{Z}_C - W}{V_R} \tag{1}$$

2.1 COMPLETE MODEL

The non linear equations describing the launcher motion are the following:

$$\begin{aligned} m\ddot{Z}_C &= -P_C \sin(\beta+\theta) - qS_{ref}C_{n\alpha}\alpha\cos\theta + qS_{ref}C_{xmin}\sin\theta & (2)\\ J\ddot{\theta} &= J\dot{q} = -P_C|TG|\sin\beta + qS_{ref}C_{n\alpha}\alpha\overline{GR} + qS_{ref}L_{ref}C_{m\alpha}\alpha & (3)\end{aligned}$$

Considering these equations at the equilibrium leads to:

The linearization of the motion equations around an equilibrium state (α_0, θ_0, β_0) has been performed considering that the aerodynamic coefficients (lift, pitch and drag respectively) are formulated as follows:

$$\begin{aligned} C_n &= C_{n\alpha}(\alpha-\alpha_0) & (4)\\ C_m &= C_{m0} + C_{m\alpha}(\alpha-\alpha_0) & (5)\\ C_a &= C_{xmin} + K_{x\alpha}(\alpha-\alpha_0)^2 & (6)\end{aligned}$$

thus leading to the equilibrium state equations:

$$\begin{aligned} -P_C\sin(\beta_0+\theta_0) - qS_{ref}[C_{n0}\alpha_0\cos\theta_0 - C_{xmin}\sin\theta_0] &= 0 & (7)\\ -P_C|TG|\sin\beta_0 + qS_{ref}C_{n\alpha}\alpha_0\overline{GR} + qS_{ref}L_{ref}C_{m\alpha}\alpha_0 &= 0 & (8)\end{aligned}$$

Moreover, as the launcher is symmetric, $\alpha_0 = C_{m0} = 0$. Finally, the resulting state space representation is given by:

$$\begin{bmatrix} \dot{\theta} \\ \ddot{\theta} \\ \ddot{Z}_C \end{bmatrix} = \begin{bmatrix} 0 & 1 & 0 \\ A_6 & 0 & \frac{A_6}{V} \\ a_1 & 0 & a_2 \end{bmatrix} \begin{bmatrix} \theta \\ \dot{\theta} \\ \dot{Z}_C \end{bmatrix} + \begin{bmatrix} 0 & 0 \\ -\frac{A_6}{V} & K_1 \\ -a_2 & a_3 \end{bmatrix} \begin{bmatrix} W \\ \beta \end{bmatrix} \tag{9}$$

The output vector is then chosen as follows:

$$Y = \begin{bmatrix} \alpha \\ \theta \\ \dot{\theta} \\ \dot{Z}_C \end{bmatrix} = \begin{bmatrix} 1 & 0 & \frac{1}{V} \\ 1 & 0 & 0 \\ 0 & 1 & 0 \\ 0 & 0 & 1 \end{bmatrix} \begin{bmatrix} \theta \\ \dot{\theta} \\ \dot{Z}_C \end{bmatrix} + \begin{bmatrix} -\frac{1}{V} & 0 \\ 0 & 0 \\ 0 & 0 \\ 0 & 0 \end{bmatrix} \begin{bmatrix} W \\ \beta \end{bmatrix} \tag{10}$$

where

$$\begin{aligned} a_1 &= \frac{1}{m}\left[-P_c\cos(\theta_0+\beta_0) + qS_{ref}C_{n\alpha}\alpha_0\sin\theta_0 + qS_{ref}C_{xmin}\cos\theta_0\right] & (11)\\ a_2 &= -\frac{1}{mV_R}\left[qS_{ref}C_{n\alpha}\cos\theta_0\right] & (12)\\ a_3 &= -\frac{P_C}{m}\cos(\theta_0+\beta_0) & (13)\\ K_1 &= -\frac{P_C}{J}|TG|\cos\beta_0 & (14)\\ A_6 &= -\frac{qS_{ref}}{J}\left[C_{m\alpha}L_{ref} + C_{n\alpha}\overline{GR}\right] & (15)\end{aligned}$$

m and J are the launcher mass and inertia, S_{ref} is the reference surface, $|TG|$ is the modulus of $\overrightarrow{TG}$ and $\overline{GR}$ is the component of $\overrightarrow{GR}$ along X_C (R being the reference point where the aerodynamic coefficients are considered).

As a matter of validation, the last two parameters of the linear model A_6 and K_1 have been computed for several Mach conditions (Fig. 2) and compared to identified values from flight data (Fig. 3)

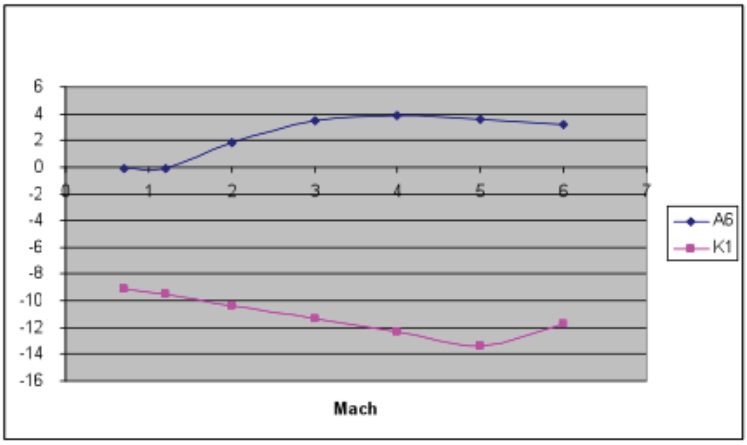

Figure 2: Computed values of A_6 and K_1

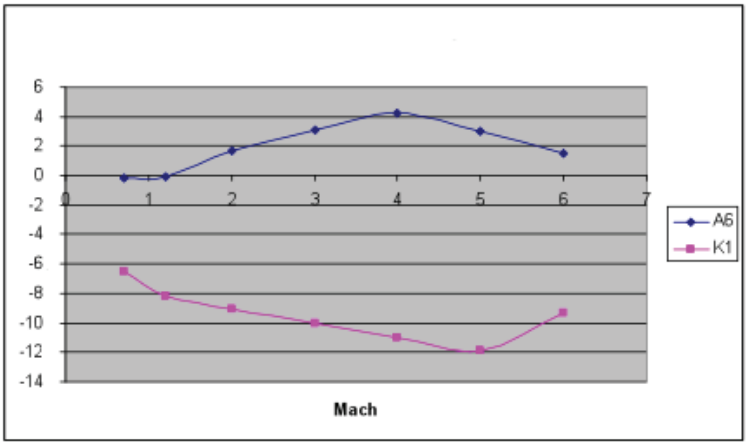

Figure 3: Identified values of A_6 and K_1

2.2 REDUCED MODEL

A modal analysis of the above linear model (9) makes clear that there is an unstable mode related to the lateral drift of the launcher ($\dot{Z}_C$). As this mode is easily stabilizable by the

guidance loop, it can be ignored at first, thus leading to a simplified or reduced model:

$$\begin{bmatrix} \dot{\theta} \\ \ddot{\theta} \end{bmatrix} = \begin{bmatrix} 0 & 1 \\ A_6 & 0 \end{bmatrix} \begin{bmatrix} \theta \\ \dot{\theta} \end{bmatrix} + \begin{bmatrix} 0 & 0 \\ -\frac{A_6}{V} & K_1 \end{bmatrix} \begin{bmatrix} W \\ \beta \end{bmatrix}$$
$$\begin{bmatrix} \alpha \\ \theta \\ \dot{\theta} \end{bmatrix} = \begin{bmatrix} 1 & 0 \\ 1 & 0 \\ 0 & 1 \end{bmatrix} \begin{bmatrix} \theta \\ \dot{\theta} \end{bmatrix} + \begin{bmatrix} -\frac{1}{V} & 0 \\ 0 & 0 \\ 0 & 0 \end{bmatrix} \begin{bmatrix} W \\ \beta \end{bmatrix} \tag{16}$$

3 CONVENTIONAL CONTROL OF THE ANGLE OF ATTACK

The desired performances, for every flight scenario, can be summarized as follows:

- gain margin at high frequency: $5dB$
- gain margin at low frequency: $2dB$
- phase margin: $25deg$
- minimal damping ratio: 0.5
- closed loop bandwidth equal to the natural frequency of the launcher ($\sqrt{A_6}\ s^{-2}$ from the linear model)

The operating point considered along the trajectory to derive the linear model has been chosen where the dynamic pressure is maximum, which corresponds to the most critical situation in terms of stability margins. The linear controller is then tuned for this particular point with respect to the above specifications, and finally applied to the whole trajectory. The controller is basically a PD type controller with a feedforward gain h applying on the reference signal α_c to ensure a unity gain:

$$\beta = K_p(h\alpha_c - \alpha) - K_v\dot{\alpha} \tag{17}$$

If we consider that the angle of attack α is not measured (only the pitch angle θ is measured), that the lateral deviation $\dot{Z}_C$ is available from the guidance loop, the control law (17) can be modified, also adding an integral term and a pseudo derivative, thus becoming:

$$\beta = (K_p + \frac{K_i}{s}) \left[h\alpha_c - (\theta + \frac{\dot{Z}_C}{V}) \right] - K_v \frac{s}{1+\tau s}\theta \tag{18}$$

Even if it has resulted quite easy to tune this controller for the chosen operating point, a more realistic simulation of the control scheme (18), including the servo dynamic and the global time delay (Fig. 4) has exhibited poor performances for several operating points along the trajectory. In particular, we noted a badly dominant mode and a too weak phase margin. Thus the main controller parameters (K_p, K_v, h and τ the time constant of the pseudo derivative) have been tuned over several operating points and then interpolated.

Simulation results are presented on Fig. 5, showing good behavior either for reference tracking or disturbance rejection. The simulation is limited to the first 3 seconds as the unstable mode (lateral deviation) is not controlled yet.

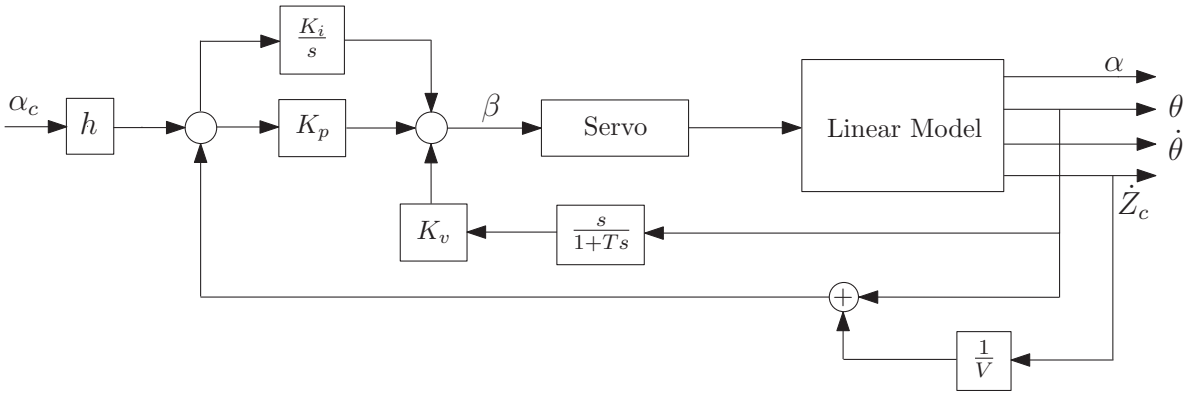

Figure 4: Control of the angle of attack

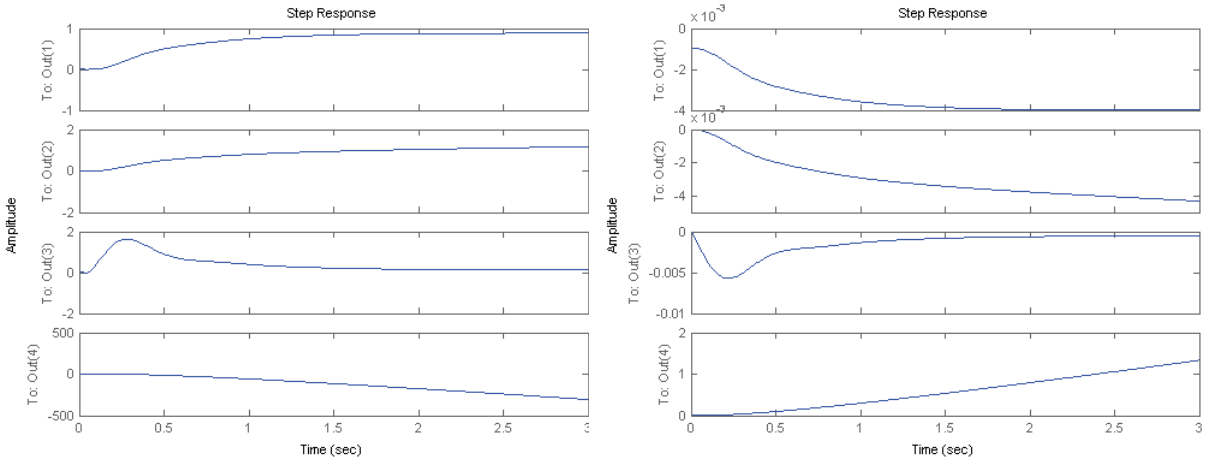

Figure 5: Step responses from α_c (left) and wind W (right). Top to bottom : α, θ, $\dot{\theta}$, $\dot{Z}_C$.

4 Linear Fractional representation of the microlauncher

4.1 Position of the problem

The key principle of the Linear Fractional Representation (LFR) is to describe a Linear Parameter Varying (LPV) system using the well known $M - \Delta$ interconnection (Fig. 6). where

- $M = \begin{bmatrix} M_{11} & M_{12} \\ M_{21} & M_{22} \end{bmatrix}$ is the LFR model
- $\Delta = \begin{bmatrix} \delta_1 \mathbb{I}_{n1} & 0 & \cdots \\ 0 & \delta_2 \mathbb{I}_{n2} & \cdots \\ \vdots & \vdots & \ddots \end{bmatrix}$ is the uncertainty block where every varying parameter δ_i is repeated ni times.

The input-output relation is then given by:

$$y = [M_{22} + M_{21}\Delta(\mathbb{I} - M_{11}\Delta)^{-1}M_{12}]u \tag{19}$$

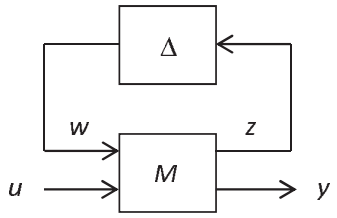

Figure 6: $M - \Delta$ representation

	A_6	K_1	a_1	a_2	a_3	V	LFR model
size of $Mach$ block	3×3	3×3	7×7	5×5	3×3	1×1	22×22
size of $Pdyn$ block	2×2	2×2	3×3	2×2	2×2	1×1	12×12

Table 1: Dimensions of the uncertainty blocks from the first approach

The LFT is thus entirely defined by M, the orders ni, and the bounds of every varying parameter δ_i (usually normalized).
The starting point is the choice of the physical parameters that should be used to characterize the different trajectories. An exhaustive work led to the conclusion that both Mach number ($Mach$) and dynamic pressure ($Pdyn$) were the more appropriate parameters, allowing to cover the different flight trajectories. Thus the *LFR Control Toolbox* has been exploited to generate an LFR model of the microlauncher. More specifically, we used the `grid2lfr` function that allows to find the coefficients of a rational expression defined in term of $Mach$, $1/Mach$, $Pdyn$ and $1/Pdyn$ with user defined orders: Concretely, it performs a least squares based interpolation of a varying parameters matrix for several points of the $Mach$-$Pdyn$ plane.

4.2 First approach

For this first approach, every parameter present in the linear model (9) is considered separately: 6 LFR objects are created (for A_6, K_1, a_1, a_2, a_3 and V) and then assembled using the linearized equations of (9).
As an illustration, the LFR of two parameter (A_6 and K_1) are plotted in the ($Mach$, $Pdyn$) plane for several trajectories (Figs. 7 and 8): despite relative low orders, the LFR approximations remain close to the real values, especially for A_6.

Once the 6 LFR have been computed, the overall LFR model has been built using the state equations governing the linear dynamics (9), resulting in a block diagram scheme given in Fig. 9. It has to be noticed that every parameter is only used once in such a scheme, and that the resulting LFR object is characterized by an uncertainty block Δ where $Mach$ is repeated 22 times and $Pdyn$ 12 times (Table 1).

Finally, the LFR model has been validated comparing LTI models computed for several operating conditions and the corresponding LTI models obtained from the above LFR object.

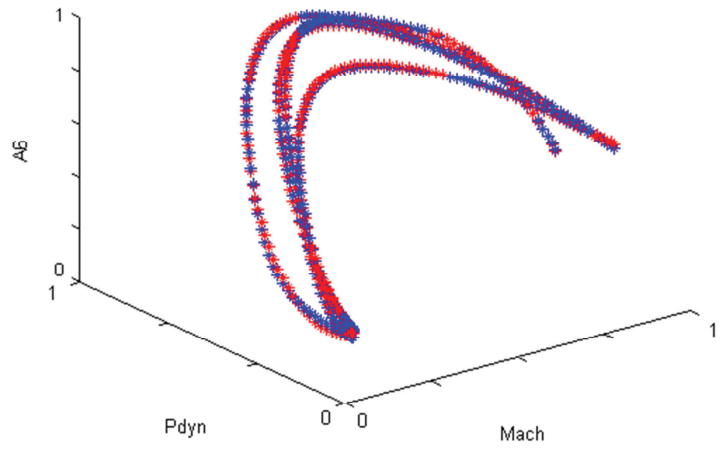

Figure 7: A_6 parameter (blue) and its LFR approximation (red); Normalized values.

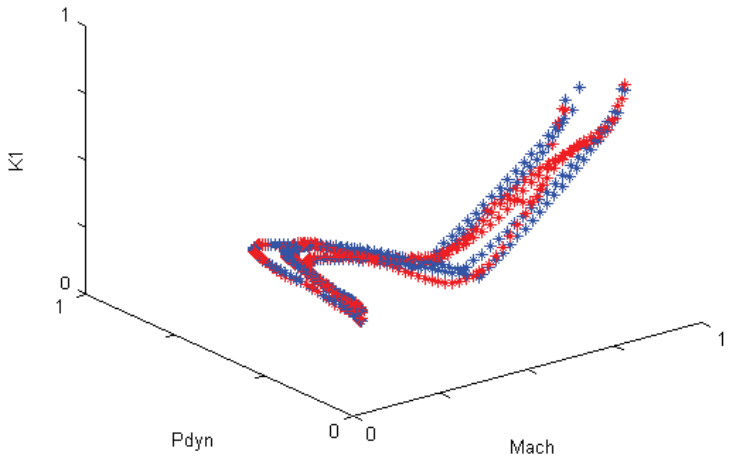

Figure 8: K_1 parameter (blue) and its LFR approximation (red); Normalized values.

4.3 Second approach

Instead of considering each single parameter as previously, one can consider a parameter matrix M formed from the linear model (9):

$$M = \begin{bmatrix} A_6 & A_6/V & K_1 \\ a_1 & a_2 & a_3 \\ 1 & 1/V & 0 \end{bmatrix} \tag{20}$$

Indeed, the scheme presented in Fig. 9 can also be represented by the new block diagram given in Fig. 10.

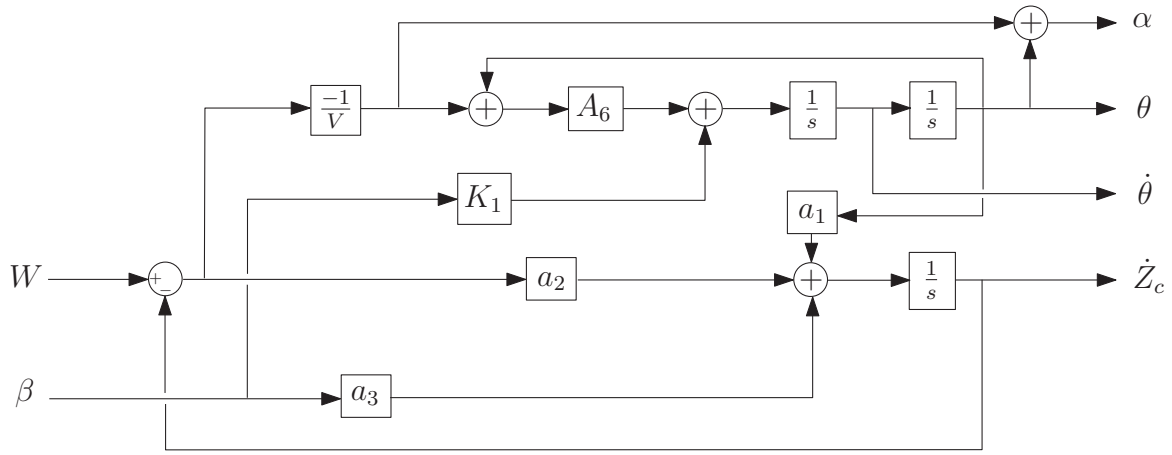

Figure 9: Construction of the LFR model (every LFR gain is used once)

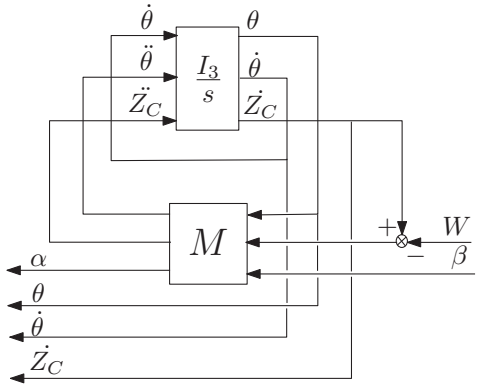

Figure 10: Construction of the LFR model from the LFR matrix M.

Even if this method is globally less accurate in terms of approximation, its main advantage lies in the size of the generated Δ block: $Mach$ and $Pdyn$ are repeated 12 times, which is a better solution than the one generated by the first approach.

5 LPV synthesis based Controller design

In [6] and [7] a general H_∞ design based on the acceleration sensitivity function was proposed to control mechanical systems taking into account specifications on disturbances rejection performance and dynamic decoupling between degrees of freedom (d.o.f.). This particular H_∞ standard problem is also called the SOTAS (Second-Order Template on Acceleration Sensitivity function) problem.

The algorithm that is used to solve this robust LPV control design problem is in fact an algorithm of robust synthesis. Thus it allows the synthesis of linear controller maximizing the worst performance index obtained over the whole uncertainty domain, which can be represented by finding K in the interconnection of Fig. 11. Indeed, we are here looking for a LPV controller maximizing the robust performance of an uncertain LPV standard-form. In fact, the robust LPV control design problem can be rewritten as a robust control design problem of a static controller. Control design is performed with a robust control algorithm proposed by [8]. This method uses

an iterative resolution of a Linear Matrix Inequalities (LMI) problem as an heuristic to address a Bilinear Matrix Inequality (BMI) derived from the Kalman-Yakubovic-Popov (KYP) lemma. It allows simultaneous robust and fixed-order synthesis of both a feedback controller and a feedforward controller under LTI and LTV uncertainties.
Then the starting point of the above mentioned method consists in finding a stabilizing initial controller K_0. In our case, we chose $K_0 = 0.5\frac{1+0.2s}{1+0.01s}$, i.e. a simple lead phase controller.

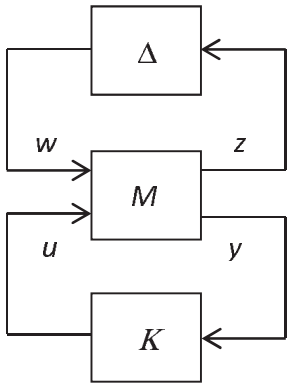

Figure 11: Standard form for robust control design

The application of such a technique to our problem is detailed in Fig. 12, where both servo dynamics and propagation delays have been included. Only the reduced model of the launcher (16) has been considered. The synthesis has been performed in the continuous time domain. Then the resulting LPV controller has been discretized. Parameters ω and ξ specify the required bandwidth and damping ratio for the dominant closed loop modes.

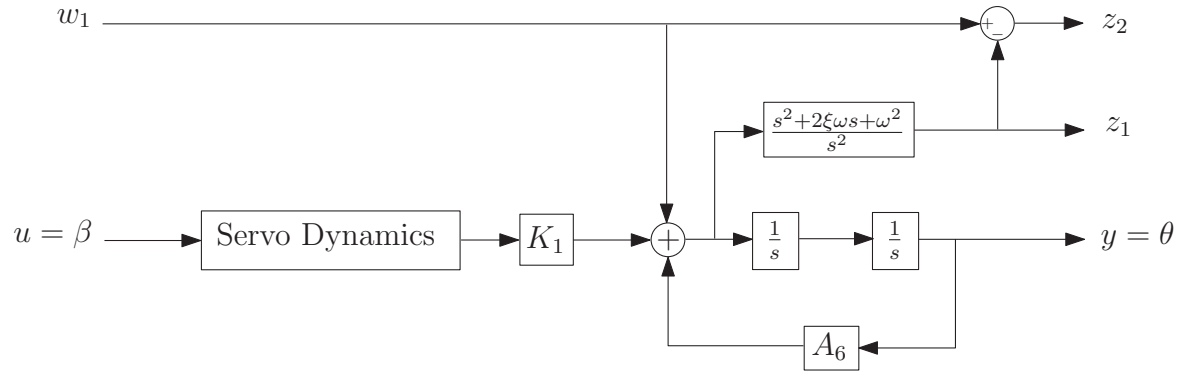

Figure 12: LPV control design formulation

As an illustration of the obtained solution, The controller Bode diagram is reported on Fig. 13 while the open loop Black chart is reported on Fig. 14. The Bode charts exhibit homogeneous characteristics, whatever the flight point that is considered, and always close to the initial controller. Moreover, Fig. 14 shows that stability is ensured, even if the stability margins slightly decrease (as expected) when considering the discretized controller.

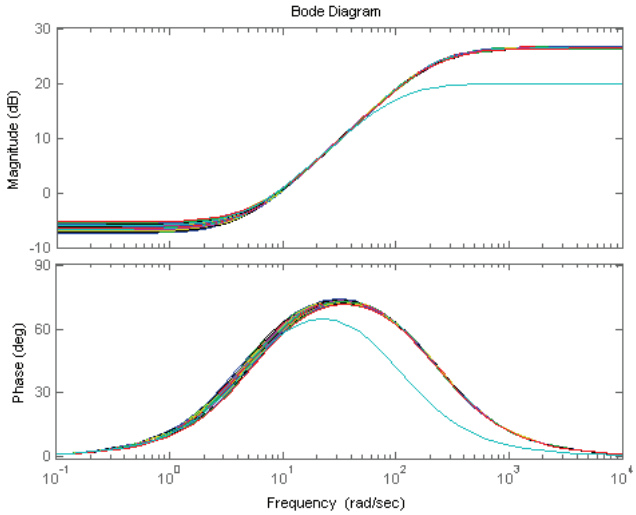

Figure 13: Bode plot of the LPV controller for several flight points (initial controller K_0 in cyan)

6 LFT representation of the conventional controller

In section 3 the conventional control law (18) gains (K_p, K_v, h) have been tuned for several flight points and then interpolated. Here we consider another solution that consists in finding a LFT for every gain as functions of $Mach$ and $Pdyn$ parameters. To build the LFT of each controller gain, we considered the interpolated values every second along the trajectory. As previously, we used the LFR Toolbox and more specifically the function `grid2lfr`. We can note that although the specified orders for the 3 LFT remain small, the resulting LFT exhibit high dimensions. For instance, for the resulting K_p LFT, the Δ block dimension is 8: $Mach$ and $Pdyn$ are repeated 5 times and 3 times respectively.

Figures 15, 16 and 17 depict the evolution of the 3 gains in the $Mach$-Pyn plane, comparing the LFT model and the interpolated values. It appears that for both K_p and K_v there are significative differences, but not for h. Anyway, as a matter of validation, the evaluation of K_p and K_v at $t = 25s$ for instance lead to the following results:

- $K_p = -0.3887$ from the LFT model and $K_p = -0.4045$ from the interpolation
- $K_v = -0.0800$ from the LFT model and $K_v = -0.0788$ from the interpolation

which is acceptable.

7 Simulation results

7.1 Structure of the simulation environment

In order to compare the 3 control laws developed earlier, the simulation of the microlauncher has been improved to reach a high level of fidelity. The overall simulation scheme is given on Fig. 18. Its main characteristics are the following:

- non stationary simulation of the microlauncher: it is realized via *continuous* computations of the linear model (9).

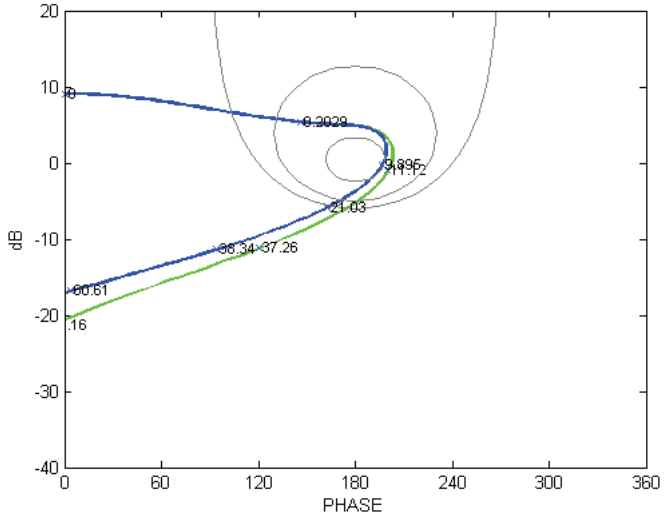

Figure 14: Open loop Black plot (continuous in green, discretized in blue)

- stabilization of the lateral deviation: the $\dot{Z}_c$ mode is simply stabilized with a roughly tuned PID controller.
- disturbance rejection type: only the wind input is considered ($\dot{Z}_{cref}$ set to zero). Wind shears are simulated in a realistic way from real data.

Moreover, as the angle of attack α is not measured, it is replaced by its approximate (or estimated) value (6):

$$\widehat{\alpha} = \theta + \frac{\dot{Z}_C}{V_R} \tag{21}$$

7.2 Comparison of the control laws

As a reminder, the 3 control laws developed during this work are:

- Conventional control law (18), referred as **L1**. Taking into account that the integral term is set to zero, that this control law is sampled (sampling period T_s), and that the gains are interpolated, its expression becomes:

$$\beta(t) = K_p(t)\left[h(t)\alpha_c - (\theta + \frac{\dot{Z}_C}{V})\right] - K_v(t)\frac{z-1}{T_s z}\theta \tag{22}$$

- LFT conventional control law, referred as **L2**: As explained in section 6, the same control law (22) is considered, but replacing the gains $K_p(t)$, $K_v(t)$ and $h(t)$ by their corresponding LFT representations.
- LFT controller, referred as **L3**: the frequency behavior of this controller, designed in section 5, is given on Fig. 13 and Fig. 14.

The 3 control laws implementation are finally detailed on figures 19, 20 and 21, and the corresponding simulation results are presented on figures 22, 23 and 24.

From these results, some particular points can be underlined:

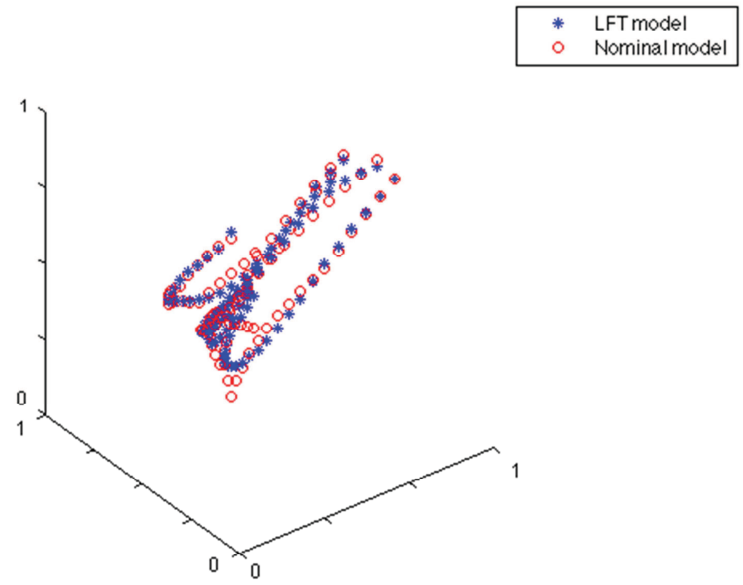

Figure 15: LFT representation of K_p versus normalized $Mach$ and $Pdyn$

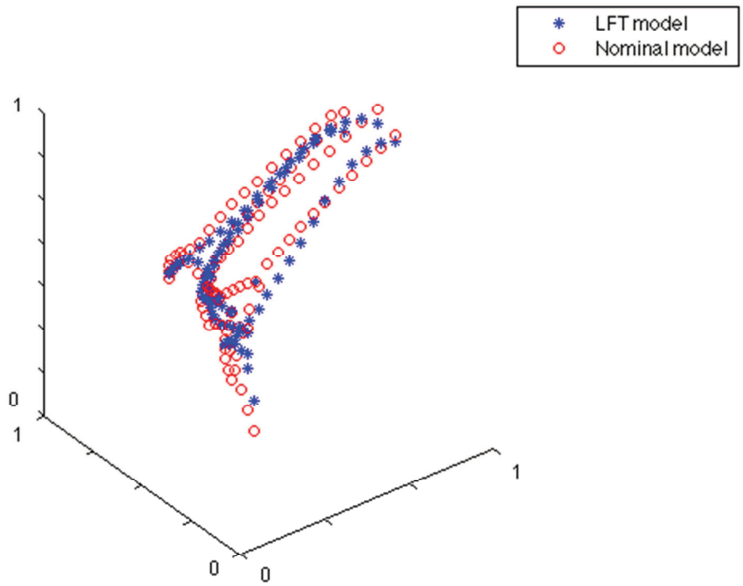

Figure 16: LFT representation of K_v versus normalized $Mach$ and $Pdyn$

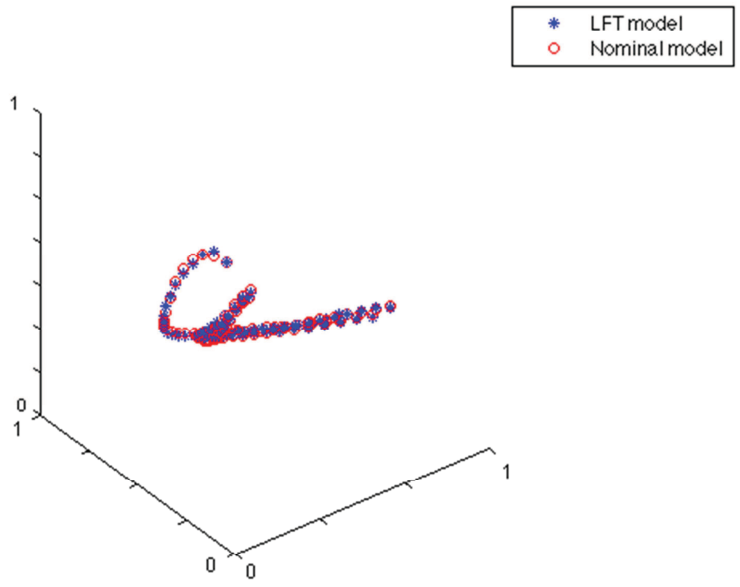

Figure 17: LFT representation of h versus normalized $Mach$ and $Pdyn$

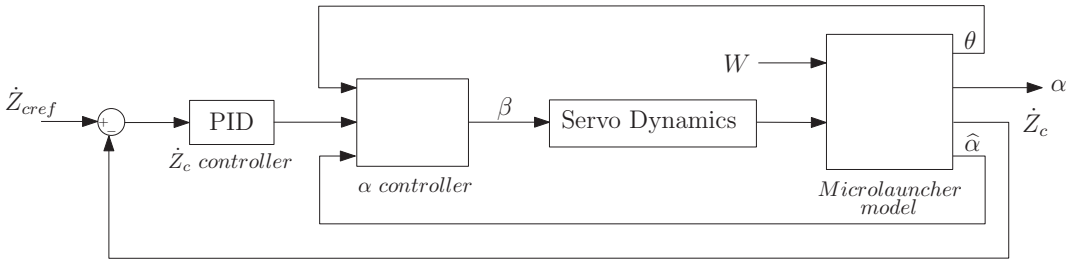

Figure 18: Overall control scheme

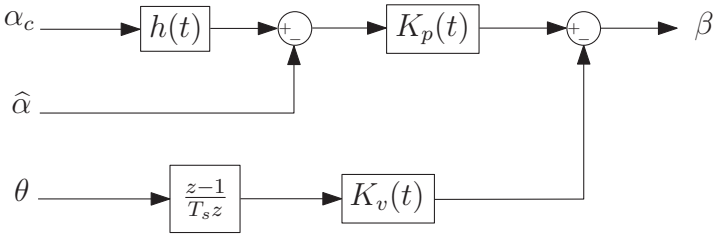

Figure 19: Implementation of L1 control law

- The initial oscillations of the actuator (L1 and L2 control laws) are due to a badly tuned guidance controller (PID for $\dot{Z}_C$). In fact this PID has been tuned at an operating point situated at the half trajectory (around 20s), thus not adapted to the initial trajectory.
- The divergence of the L1 control law is more problematic. It corresponds to the end of the trajectory, characterized by a highly decreasing thrust thus leading to highly varying gains. This phenomenon causes an instability for L1, but not for L2 because the LFTs of

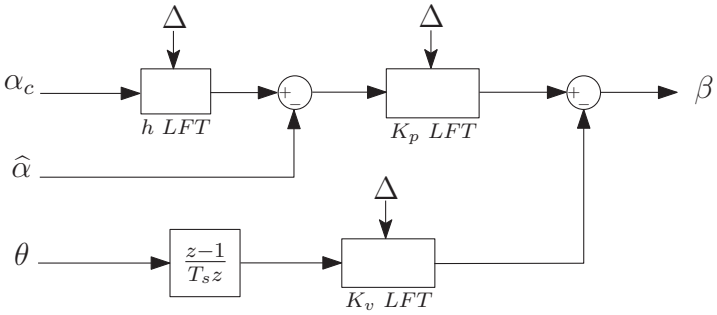

Figure 20: Implementation of L2 control law

![!h]

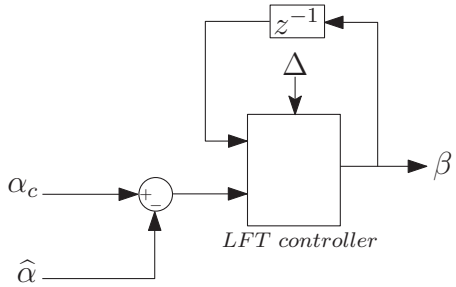

Figure 21: Implementation of L3 control law

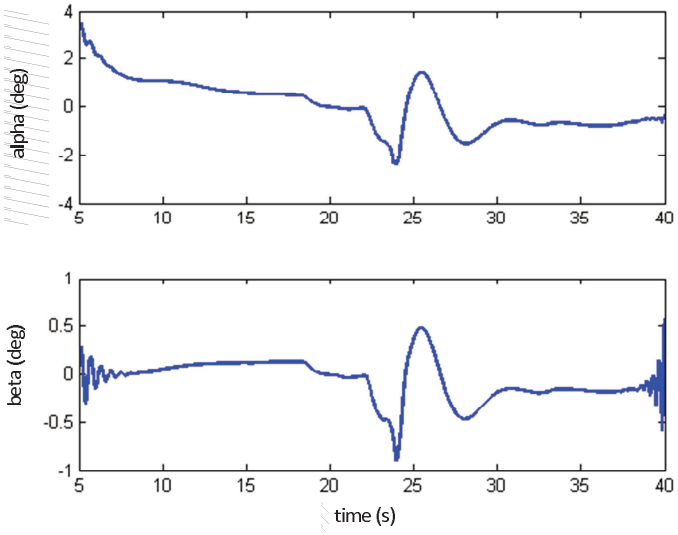

Figure 22: Evolution of α and β in response to wind disturbances: control law L1

the 3 gains did not take into account the ending gains.

- The L3 control law exhibits a better behavior at the origin of the trajectory, while remaining stable along the whole trajectory.

Moreover, frequency and step responses have been simulated for every control law and considering many operating points along the trajectory. It clearly appears that the desired stability

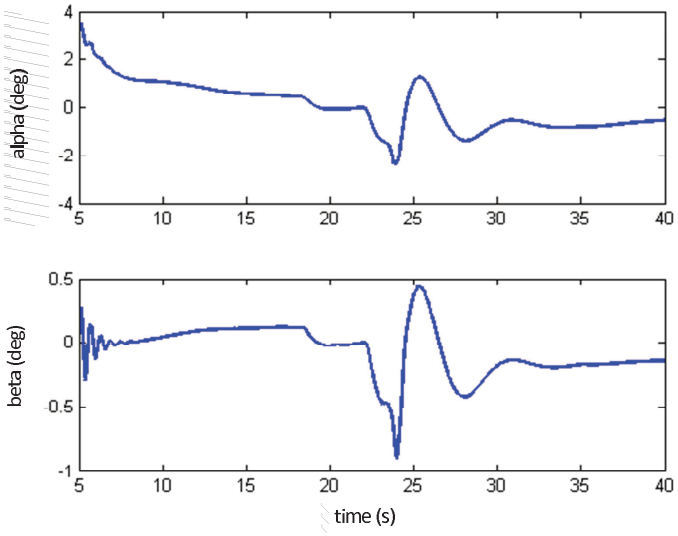

Figure 23: Evolution of α and β in response to wind disturbances: control law L2

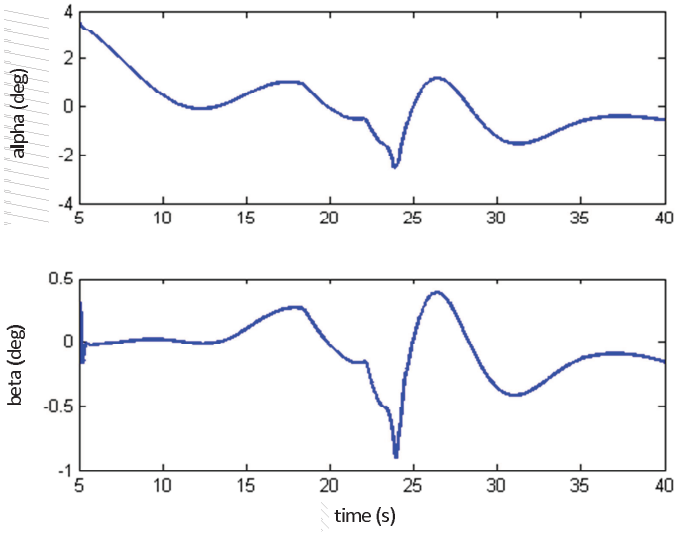

Figure 24: Evolution of α and β in response to wind disturbances: control law L3

margins are obtained ($2dB$ and $5dB$ gain margins, $25deg$ phase margin). Anyway, the L2 control law exhibit slightly better results in terms of stability margins, but L3 seems more robust with respect to step responses.

8 Conclusion

In this work, the problem of controlling the angle of attack of a micro-launcher has been addressed. It has been shown that the choice of the Mach number and the dynamic pressure led to a reasonably complex and representative LPV model of the launcher. However, this choice is not unique and others parameters could be considered. The controller design has been performed

using two competitive methods that gave satisfactory simulation results. As expected, the main limitation lies in the size of the uncertainty block Δ, but the proposed solution allows to reach a good balance between computational complexity and performances satisfaction.

References

[1] Marcos A, Balas G.J. *Development of linear parameter varying models for aircraft*, *AIAA J. Guid., Control Dyn.*, vol. 27, no. 2, pp. 218228, 2004.

[2] Szabò Z, Marcos A, Mostaza Prieto D, Kerr M.L, Rodonyi G, Bokor J, Bennani S. *Development of an integrated LPV/LFT framework: Modeling and data-based validation tool*, *IEEE Trans. on Control Systems Technology*, vol. 19, no. 1, pp. 104-117, January 2011.

[3] Fezans N, Alazard D, Imbert N, Carpentier B. *H_∞ control design for multivariable mechanical system - Application to RLV reentry. Proceedings of the 2007 AIAA Guidance, Navigation, and Control Conference and Exhibit*, AIAA, Hilton Head Island, SC, pp. 1-13, August 2007.

[4] Magni J.F, *User Manual of the Linear Fractional Representation Toolbox Version 2.0* Technical report, ONERA - Systems Control and Flight Dynamics Depertment, October, 2005. (http://http://www.onera.fr/staff-en/jean-marc-biannic)

[5] Ferrères G, Biannic J.M, *Introduction to a Simulink-based interface for LFRT Toolbox* (http://www.cert.fr/dcsd/idco/perso/Biannic/toolboxes.html/slklfr)

[6] Fezans N, Alazard D, Imbert N, Carpentier B. *H_∞ control design for generalized second order systems based on acceleration sensitivity function*, *Proceedings of the 16^{th} Mediterranean Conference on Control and Automation*, June 2008.

[7] Fezans N, Alazard D, Imbert N, Carpentier B. *Mixed H_2/H_∞ control design for mechanical systems: analytical and numerical developments*, *Proceedings of the 2008 AIAA Guidance, Navigation, and Control Conference and Exhibit*, Hawai, USA, August 2008.

[8] Roos C, Biannic J.M. *A positivity approach to robust controllers analysis and synthesis versus mixed LTI/LTV uncertainties*, *Proceedings of the American Control Conference*, Minneapolis, Minnesota, pp. 3661-3666, June 2006.